Available online at www.sciencedirect.com
ScienceDirect
Journal of Computational and Applied Mathematics 204 (2007) 209–218
JOURNAL OF COMPUTATIONAL AND APPLIED MATHEMATICS
www.elsevier.com/locate/cam

High order Hybrid central—WENO finite difference scheme for conservation laws

Bruno Costa[a], Wai Sun Don[b,*]

[a] *Departamento de Matemática Aplicada, IM-UFRJ, Caixa Postal 68530, Rio de Janeiro, RJ, C.E.P. 21945-970, Brazil*
[b] *Division of Applied Mathematics, Brown University, Providence, RI 02912 Providence, Rhode Island 02912, USA*

Received 20 July 2005; received in revised form 30 January 2006

Abstract

In this article we present a high resolution hybrid central finite difference—WENO scheme for the solution of conservation laws, in particular, those related to shock–turbulence interaction problems. A sixth order central finite difference scheme is conjugated with a fifth order weighted essentially non-oscillatory WENO scheme in a grid-based adaptive way. High order multi-resolution analysis is used to detect the high gradients regions of the numerical solution in order to capture the shocks with the WENO scheme while the smooth regions are computed with the more efficient and accurate central finite difference scheme. The application of high order filtering to mitigate the dispersion error of central finite difference schemes is also discussed. Numerical experiments with the 1D compressible Euler equations are shown.

Keywords: Central finite difference; WENO; Multi-resolution; Hybrid; Conservation laws

1. Introduction

Direct numerical simulation of turbulent flows requires very accurate numerical schemes with the ability to resolve both large and small eddies that are often at wavelengths differing several orders of magnitude from each other. High order central finite difference (CeFD) schemes are straightforward, easy to implement, and sufficiently accurate to capture the smallest resolvable scales presented at these problems with a small number of points per wavelength. Many such high order finite difference schemes had been discussed and deployed for solving linear advection problems such as the Maxwell equations in electro-magnetics and wave equations in Acoustics [17,4].

Another important issue appears when dealing with the modeling of compressible flows via the inviscid Euler equations due to the spontaneous appearance of finite time singularities. When applied to such problems, fixed stencil explicit schemes like central finite difference schemes produce oscillations that do not decrease in size with grid refinement. This so-called Gibbs Phenomenon causes loss of accuracy and, if not properly controlled by means of artificial dissipation, instability might follow as a consequence of the contamination of the solution by these oscillations. Essentially non-oscillatory (ENO) schemes [14,15] have been developed in order to overcome the Gibbs phenomenon. ENO schemes make use of nonlinear weights based on divided differences of the numerical solution in order to bias

* Corresponding author.
E-mail addresses: bcosta@ufrj.br (B. Costa), wsdon@cfm.brown.edu (W.S. Don).

0377-0427/$ - see front matter © 2006 Elsevier B.V. All rights reserved.
doi:10.1016/j.cam.2006.01.039

the local stencils when computing derivatives, avoiding interpolations across discontinuities. Weighted essentially non-oscillatory (WENO) schemes [11,13] are an improvement over ENO schemes due to their higher order of accuracy with same stencil size. A convex combination of all the possible sub-stencils of ENO achieves optimal order of accuracy at the smooth parts of the solution. Nevertheless, the intrinsic numerical dissipation of WENO schemes, although necessary to properly capture shock waves, might seriously damp relevant small scales.

A natural idea is then to conjugate shock capturing schemes, to be applied around discontinuities, with high order central finite difference methods for the smooth parts of the solution. In this article, we study the conjugation of high order central finite difference and WENO schemes when numerically solving systems of hyperbolic conservation laws. One important component is a switch algorithm to dynamically decide, at any given time step, which scheme to turn on at each grid point. The switch we apply is based on Ami Harten's work [7,8], where a high order multi-resolution (MR) analysis is performed at every step of the temporal integration process. The resulting adaptive scheme ensures that fluxes at grid points around discontinuities will always be computed by a WENO scheme, where as smooth tendencies will not suffer any unnecessary extra damping since they will be treated by a CeFD scheme. Another advantage is that the application of the CeFD scheme avoids the heavy machinery employed by the characteristic-wise WENO finite difference algorithm such as the evaluation of the Jacobian of the fluxes, characteristics decomposition and recomposition and the global Lax–Friedrichs flux splitting.

In this work, we will focus on the maximum order central finite difference scheme. Other standard and dispersion optimized central finite difference schemes can be employed [17] but will not be explored in this study at this time. Due to the non-dissipative nature of the central finite difference scheme, the inherent dispersion error, although small, generates undesirable oscillations polluting the solution in time. By applying high order filtering [16] we are able to mitigate grid-size oscillations that, otherwise, would destroy the accuracy.

The paper is organized as follows: In Section 2 we briefly introduce the WENO finite difference scheme. Section 3 presents Harten's MR algorithm. A brief discussion on the central finite difference scheme is given in Section 4. The Hybrid scheme is presented in Section 5. Numerical experiments with the proposed Hybrid scheme for the one-dimensional Mach 3 shock-entropy wave interaction are shown in Section 6. The conclusions are given in Section 7.

2. ENO and WENO schemes

In this section we describe the ENO and WENO schemes for one-dimensional scalar conservation laws:

$$u_t + f(u)_x = 0. \tag{1}$$

The conservative finite difference formulation of (1) in a uniformly spaced grid is

$$\frac{\mathrm{d}u_i(t)}{\mathrm{d}t} = -\frac{1}{\Delta x}(\hat{f}_{j+1/2} - \hat{f}_{j-1/2}), \tag{2}$$

where Δx is the grid size, $u_i(t)$ is the solution within the stencil $I_i = [x_{i-1/2}, x_{i+1/2}]$ and the numerical flux

$$\hat{f}_{i+1/2} = \hat{f}(u_{i-r}, \ldots, u_{i+s}), \tag{3}$$

with r and s, integer parameters defining the set of values used for the computation of the flux $f(u)$, satisfies the following conditions:

- $\hat{f}$ is a Lipschitz continuous function in all arguments;
- $\hat{f}$ is consistent with the physical flux f, i.e., $\hat{f}(u, u, \ldots, u) = f(u)$.

Thus, the Lax–Wendroff theorem applies, and the conservative solution from (2), if it converges, will converge to a weak solution.

The following problem is related to the computation of the numerical flux $\hat{f}$ above:
Given $v_i = v(x_i)$, find $\hat{v}_{i+1/2} = \hat{v}(v_{i-r}, \ldots, v_{i+s})$ such that

$$\frac{1}{\Delta x}(\hat{v}_{i+1/2} - \hat{v}_{i-1/2}) = v'(x_i) + \mathrm{O}(\Delta x^k). \tag{4}$$

In other words, it is desired that the flux difference above be a kth order approximation to the derivative of v. This can be accomplished by means of an auxiliary function $h(x)$ which can be implicitly defined as

$$v(x) = \frac{1}{\Delta x}\int_{x-\Delta x/2}^{x+\Delta x/2} h(\xi)\,\mathrm{d}\xi. \tag{5}$$

Since

$$v'(x_i) = \frac{1}{\Delta x}(h_{i+1/2} - h_{i-1/2}), \tag{6}$$

we take

$$\hat{v}_{i+1/2} = h_{i+1/2} + \mathrm{O}(\Delta x^k), \tag{7}$$

and the problem is solved.

We are now left with the problem of finding a kth order approximation for $h(x)$. We start by noticing that, as defined above, $\{v_i\}$ are the cell averages of $h(x)$ in the intervals I_i. Therefore, the primitive function of $h(x)$ can be defined as $H(x) = \int_{-\infty}^{x} h(x)\,\mathrm{d}x$ and the exact values of $H(x)$ at $x_{i+1/2}$ are $H(x_{i+1/2}) = \Delta x \sum_{j=-\infty}^{i} v_j$. By interpolating $H(x)$ at these values, one can find a $k+1$ degree interpolating polynomial $P(x)$. Thus, the derivative $p(x) = P'(x)$ is the desired kth order approximation of $h(x)$ we are looking for. Thus,

$$\hat{v}_{i+1/2} = p_i^r(x_{i+1/2}) = \sum_{j=0}^{k-1} c_{rj}\, v_{i-r+j} = h(x_{i+1/2}) + \mathrm{O}(\Delta x^k), \quad r = 0, \ldots, k-1, \tag{8}$$

where the coefficients c_{rj} are obtained through a Lagrangian interpolation process (see [11]). They depend on the order k of approximation and also on the left-shift parameter r, but not on the values v_i. Since r can vary from 0 to $k-1$, we have k distinct interpolating polynomials to choose from; all of them yielding a kth order approximation, once v is smooth inside the intervals considered. The above process is called the reconstruction step, for it reconstructs the values of $h(x_{i+1/2})$ at the cell boundaries from the cell average values $h(x)$ in the interval $S_r = \{\bigcup_{j=0}^{k-1} I_{i-r+j}, r = 0, \ldots, k-1\} = \{x_{i-r}, \ldots, x_{i+s}\}$ with $s = k-r-1$.

The key idea of a kth order ENO scheme [15] is to use the smoothest stencil S_r among the k candidates in order to avoid Gibbs oscillations near shocks. ENO chooses the parameter r in a way that no discontinuity is inside the intervals of the stencil S_r. However, in smooth regions all stencils together carry information for an approximation of order higher than r. WENO is an improvement over ENO for it uses a convex combination of all available polynomials for a fixed k, assigning essentially zero weights to stencils containing discontinuities. This yields a $(2k-1)$ order method at smooth parts of the solution. The flux $\hat{f}_{i+1/2}$ of the WENO method is defined as

$$\hat{f}_{i+1/2} = \sum_{r=0}^{k-1} \omega_r\, p_i^r(x_{i+1/2}). \tag{9}$$

The ENO property is obtained by requiring that the weights ω_r reflect the relative smoothness of f:

$$\omega_r = \frac{\alpha_r}{\sum_{l=0}^{k-1}\alpha_l} \quad \text{with} \quad \alpha_r = \frac{C_r}{(\varepsilon + IS_r)^\beta}, \tag{10}$$

where $\beta = 2$ and C_r are the ideal weights (see [2,11]). The parameter ε is set to 10^{-10}. A good review of the role of ε in the accuracy of the WENO scheme can be found in a recent paper [9]. There, loss of accuracy around critical points in the classical WENO scheme was also discussed and a fix was proposed, which is also implemented in this work. IS_j is a measure of the smoothness of polynomials on the stencils S_j:

$$IS_j = \sum_{l=1}^{k-1} |\Delta x|^{2l-1} \int_{x_{j-1/2}}^{x_{j+1/2}} \left(\frac{\mathrm{d}^l}{\mathrm{d}x^l} p_j^r(x)\right)^2 \mathrm{d}x. \tag{11}$$

When the interpolation polynomial p_j^r in a given stencil S_j is smooth, the smoothness indicator IS_j is relatively much smaller than those of stencils where the polynomial has discontinuities in its first $r-1$ derivatives. Therefore, discontinuous stencils receive an essentially zero weight.

For a system of conservation laws such as the Euler equations (22), the left and right eigenvectors and eigenvalues of the Jacobian of the flux are computed via the Roe Average method. The global Lax–Friedrichs flux splitting is used to split the flux into its positive and negative components. The resulting positive and negative fluxes are then projected in the characteristic field via the left eigenvectors. Each characteristic flux value is then reconstructed according to the WENO algorithm above with one point upwinding bias at each cell boundary. The numerical flux $\hat{f}_{i+1/2}$ is obtained by projecting the reconstructed characteristic flux values back into the conservative field via the right eigenvectors of the Jacobian of the flux. The details of the algorithm can be found in [11,13].

3. Multi-resolution analysis

It is essential for the Hybrid scheme proposed in this article to measure the smoothness of the solution in a high order fashion such that the appropriate high order algorithm can be used at distinct grid points.

It is common in the literature to look at divided differences of the solution in order to indicate the presence of discontinuities at a particular grid location when such differences exceed a given tolerance. When performing the numerical calculations of Section 6, the density field will be the one used for the analysis, since not only it contains the discontinuities due to the shocks and the rarefaction waves, but also the contact discontinuities, which are present in the weak solutions of systems of conservation laws such as the Euler equations. In this work, we employ the MR algorithms in [7,8] to detect the smooth and rough parts of the solution. Consider a set of nested dyadic grids $\{G^k, 0 \leqslant k \leqslant L\}$, defined as:

Given an initial number of the grid points N_0 and grid spacing Δx_0,

$$G^k = \{x_j^k,\ j = 0, \ldots, N_k\}, \tag{12}$$

where $x_j^k = j\Delta x_k$, $\Delta x_k = 2^k \Delta x_0$, $N_k = 2^{-k} N_0$ and the cell averages $\bar{f}_j^k$ of function f at x_j^k:

$$\bar{f}_j^k = \frac{1}{\Delta x_k} \int_{x_{j-1}^k}^{x_j^k} f(x)\, \mathrm{d}x, \tag{13}$$

Let $\tilde{f}_{2j-1}^k$ be the approximation to $\bar{f}_{2j-1}^k$ by the unique polynomial of degree $2s$ that interpolates $\bar{f}_{j+l}^k$, $|l| \leqslant s$ at x_{j+l}^k, where $r = 2s+1$ is the order of approximation.

The approximation error (or multiresolution coefficients) $d_j^k = \bar{f}_{2j-1}^{k-1} - \tilde{f}_{2j-1}^{k-1}$, at the kth grid level and grid point x_j, have the property that if $f(x)$ has $p-1$ continuous derivatives and a jump discontinuity at its pth derivative as denoted by $[\cdot]$, then

$$d_j^k \approx \begin{cases} \Delta x_k^p [f^{(p)}] & \text{for } p \leqslant r, \\ \Delta x_k^r f^{(r)} & \text{for } p > r. \end{cases} \tag{14}$$

The approximation error d_j^k measures how close the data at the finer grid $\{x_j^{k-1}\}$ can be interpolated by the data at the coarser grid $\{x_j^k\}$. From formula (14) it follows that

$$|d_{2j}^{k-1}| \approx 2^{-\bar{p}} |d_j^k| \quad \text{where } \bar{p} = \min\{p, r\}, \tag{15}$$

which implies that away from discontinuities, the MR coefficients $\{d_j^k\}$ diminish in size with the refinement of the grid at smooth parts of the solution; close to discontinuities, they remain at the same size, independent of k.

The MR coefficients $\{d_j^k\}$ were used in [8] in two ways. First, finer grid data $\bar{f}_j^0$ were mapped to its multiresolution representation $\bar{f}_M = (\{d_j^1\}, \ldots, \{d_j^L\}, \bar{f}^L)$ to form a multiscale version of a particular scheme, where truncation of small quantities with respect to a tolerance parameter $\varepsilon_{\mathrm{MR}}$ decreased the number of operations at fluxes computation. Secondly, the MR coefficients $\{d_j^k\}$ were also used to generate a shock detection mechanism and an adaptive method was designed where a second-order Lax–Wendroff scheme was locally switched to a first-order accurate TVD Roe

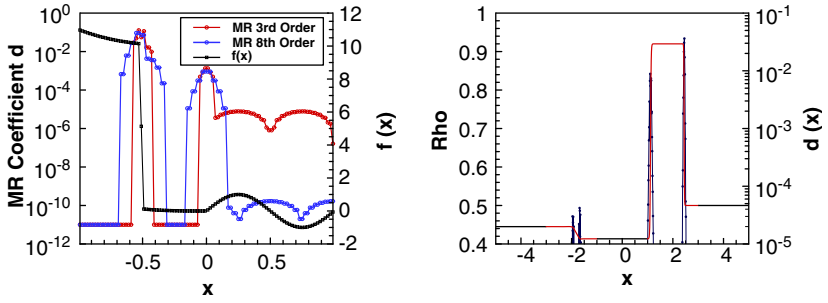

Fig. 1. Multi-resolution analysis of (left) the test function (16) and (right) the Lax problem.

scheme, whenever $\{d_j^1\}$ was larger than the tolerance parameter. In this article, we employ the latter idea where a high order central finite difference scheme is switched to a high order WENO scheme whenever a "sensor", represented by the $\{d_j^k\}$, detects discontinuities at any grid point. Since we will be using the first level $k = 1$ only, we shall drop the superscript 1 from the d_j^1 from here on unless noted otherwise.

The adaptive method of Harten used only the first level $\{d_j\}$ with a fixed MR order. However, (14) also indicates that the variation of the MR order can give additional information on the type of the discontinuity. For instance, consider the piecewise analytical function

$$f(x) = \begin{cases} 10 + x^3, & -1 \leqslant x < -0.5, \\ x^3, & -0.5 \leqslant x < 0, \\ \sin(2\pi x), & 0 \leqslant x \leqslant 1. \end{cases} \tag{16}$$

The test function (16) has a jump discontinuity at $x = -0.5$ and a discontinuity at its first derivative at $x = 0$ as depicted in Fig. 1 and analyzed by the third and the eighth MR orders. As shown in Fig. 1, the quantity $\{d_j\}$ at each grid point decays exponentially to zero inside each analytical piece of the function when the order of the MR is increased from third to eighth. At the discontinuity $x = 0.5$, $\{d_j\}$ is O(1) and remains unchanged despite the increase of the MR order. Similar behavior of the $\{d_j\}$ are exhibited at the derivative discontinuity at $x = 0$ with a much smaller amplitude. The extent of the eighth order MR is larger than the third order because more functional values are needed to perform the analysis at the higher order. In general, $N_{\mathrm{MR}} = 2(n_{\mathrm{MR}} + 1)$ number of functional values are needed for a given MR order n_{MR}.

Also, in Fig. 1, the density $f(x) = \rho(x)$ of the Lax shock tube problem with Riemann initial condition and the MR coefficients $\{d_j\}$ are shown. The location of the shock at $x \approx 2.5$, the contact discontinuity at $x \approx 1$ and the discontinuities at the edges of the rarefaction wave $x \approx -1.8$ and $x \approx -2$ are clearly delineated by the MR coefficients $\{d_j\}$. Higher order MR would not make any distinguishable difference here as the solution is a piecewise linear function.

Analogy between the wavelet analysis and the MR analysis is apparent, the MR coefficients $\{d_j^k\}$ are wavelet coefficients. Interested readers are referred to the seminal book by Daubechies [6] and references contained therein for a detailed exposition of MR analysis in the context of wavelet analysis.

4. Central finite differences schemes

In the following discussion, the computational grid is restricted to a uniformly spaced grid, i.e., $\{x_j = j\Delta x,\ j = 0, \ldots, N\}$, where Δx is the grid spacing. For a given data $\{f_j = f(x_j),\ j = 0, \ldots, N\}$, the first derivative of the function $(\mathrm{d}/\mathrm{d}x) f(x_j)$ can be approximated to order n using $2n + 1$ grid points $\{x_{j-n}, \ldots, x_{j+n}\}$ and its corresponding functional values $\{f_{j-n}, \ldots, f_{j+n}\}$ as

$$\frac{\mathrm{d}}{\mathrm{d}x} f(x_i) = \frac{1}{\Delta x} \sum_{j=-n}^{n} w_j f_{i+j}, \tag{17}$$

where w_j are the Lagrangian weights of the first derivative and here we assume $N \geqslant 2n + 1$.

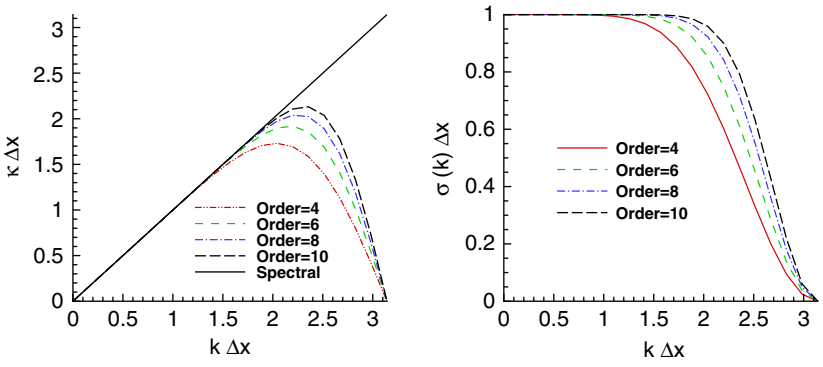

Fig. 2. The dispersion relation (left) and filter $\sigma(k\Delta x)$ (right) of central finite difference schemes of orders $n = 4, 6, 8, 10$.

One of the good properties of a central finite difference scheme is that it is non-dissipative in nature; however, dispersion is also present, requiring the use of high order smoothing. The non-dissipative property is guaranteed by requiring $w_{-j} = -w_j$. To examine its dispersive property, the Fourier transform is applied to (17), yielding the effective wavenumber κ of the scheme, which can be expressed in terms of the exact wavenumber k in the form:

$$\kappa\Delta x = 2\sum_{j=1}^{n} w_j \sin(jk\Delta x). \tag{18}$$

The difference between the effective wavenumber κ and the exact wavenumber k is the dispersion error $E(k\Delta x) = |k\Delta x - \kappa\Delta x|$. The higher the order n of the scheme, the better the scheme can resolve higher wavenumbers. However, the error analysis also indicates that the wavenumber $k = \pi/\Delta x$ can never be resolved regardless of the order of the scheme (see Fig. 2). In other words, without artificial dissipation, one can expect high wavenumbers (frequencies) error in the solution of a nonlinear hyperbolic PDE.

To mitigate dispersion error on the solution, we propose to apply high order filtering. By this, we mean that the large scales of the function are preserved up to the order of the central finite difference scheme, while the small scales, usually associated with noise and error, will be attenuated smoothly to zero.

For a given function f, discretized on a uniformly spaced grid, the filtered function $\hat{f}$ at the grid point x_i can be expressed as

$$\hat{f}_i = \sum_{j=-n}^{n} \alpha_j f_{i+j}, \tag{19}$$

where α_j are the filtering weights of order n. The filtering weights satisfy the symmetry property $\alpha_{-j} = \alpha_j$, ensuring no dispersion. The α are chosen in such a way that the first n moments of the filtered function match exactly the first n monomials $\{1, x, x^2, \ldots, x^n\}$ ensuring that the approximation order of the filtered function is kept high. In addition to that, the α are also required to satisfy the condition $\sum_{j=-n}^{n} \alpha_j (-1)^j = 0$ so that oscillations at high wavenumbers k near $\pi/\Delta x$ are attenuated to zero. By applying the Fourier transform to (19), the physical filter can be expressed as a filter $\sigma(k\Delta x)$ in the frequency space

$$\sigma(k\Delta x) = \alpha_0 + 2\sum_{j=1}^{n} \alpha_j \cos(jk\Delta x), \tag{20}$$

with $\sigma(0) = 1$ and $\sigma(\pi) = 0$ for normalization. The higher the order, the flatter is the filter near the wavenumber $k = 0$ (see Fig. 2). Therefore, more low wavenumbers remain unaltered and less higher wavenumbers get attenuated to zero. Some of these filtering weights α can be found in [16].

5. High order Hybrid central—WENO finite difference scheme

In this section, we introduce the high order Hybrid central finite difference—WENO finite difference scheme (Hybrid) for the Euler equations and discuss related issues such as the dispersion error associated with it. In this particular context, we define the Hybrid scheme as a grid-based adaptive method in which the choice of the numerical scheme is determined by the smoothness of the solution at each grid point.

Like many adaptive methods in literature, the smoothness of the solution is measured by some criteria, such as the gradient of the solution [1,12], or by the MR procedure [3,5]. A finite difference scheme such as a Compact scheme [1] or an optimized central finite difference scheme [10] can be used at those grid points where the solution is flagged as smooth in lieu of the standard high order WENO scheme. By avoiding the computationally expensive characteristics decomposition/recomposition and Jacobian evaluations of the WENO finite difference scheme, it is anticipated that the Hybrid scheme will provide greater efficiency and resolution, in particular, for large scale simulations of turbulence [10].

Here are some details of the implementation of the Hybrid scheme:

- The Hybrid scheme consists of a sixth order central finite difference scheme (CeFD6) and a fifth order WENO finite difference scheme (WENO5) for the smooth and discontinuous parts of the solution, respectively.
- The third-order three stage Runge–Kutta TVD scheme (RK3) is employed for the temporal evolution of the resulting ODE with CFL $= 0.4$ (see [11]).
- The MR analysis is applied only once at the beginning of the Runge–Kutta time stepping scheme. A grid point is flagged as non-smooth when the MR coefficient $|d_i| > \varepsilon_{\mathrm{MR}}$, a user defined MR tolerance and the WENO flux will be employed there.

$$\mathrm{Flag}_i = \begin{cases} 1, & |d_i| > \varepsilon_{\mathrm{MR}}, \\ 0 & \text{otherwise.} \end{cases} \tag{21}$$

- Once the flags are set, a number of neighboring points around each flagged point x_i, depending on the number of ghostpoints needed for a given order of the CeFD scheme and the WENO scheme, are also flagged to 1.
  In particular, if N_c and N_w are the orders of the CeFD and WENO schemes respectively, the number of ghostpoints required by CeFD and WENO schemes are $1/2N_c$ and $1/2(N_w + 1)$, respectively. At any given point, say x_i, flagged as non-smooth, its $r = \max(1/2N_c, 1/2(N_w + 1))$ neighboring points $\{x_{i-r}, \ldots, x_i, \ldots, x_{i+r}\}$ will also be designated as non-smooth, that is, $\{\mathrm{Flag}_j = 1,\ j = i - r, \ldots, i + r\}$. This procedure avoids computing the derivative of the solution by the CeFD scheme using non-smooth functional values. Furthermore, the same WENO flag will be used at all Runge–Kutta stages and will be updated at the next time step.
- Since the CeFD scheme is numerically more efficient when compared to the WENO scheme, we opt for initially computing the flux over the complete flow field with the CeFD scheme. The WENO scheme is then used to overwrite the flux at those grid points designated as non-smooth by the WENO flag.
- The class of problems studied are restricted to those where the boundary conditions do not present any complications for the ghostpoints, for instance, periodic or freestream boundary conditions. We shall use as many ghostpoints as required for the given order of the CeFD scheme, the WENO scheme and the MR analysis.

6. Numerical experiments

Let us now consider the one-dimensional Euler Equations for gas dynamics in strong conservation form:

$$\frac{\partial \vec{W}}{\partial t} + \frac{\partial \vec{F}}{\partial x} = 0. \tag{22}$$

$\vec{W} = [\rho,\ m,\ E]^{\mathrm{T}}$ is the vector of conservative variables and the flux $\vec{F}$ is given by

$$\vec{F} = \left[m,\ \frac{m^2}{\rho} + P,\ (E + P)\frac{m}{\rho}\right]^{\mathrm{T}}. \tag{23}$$

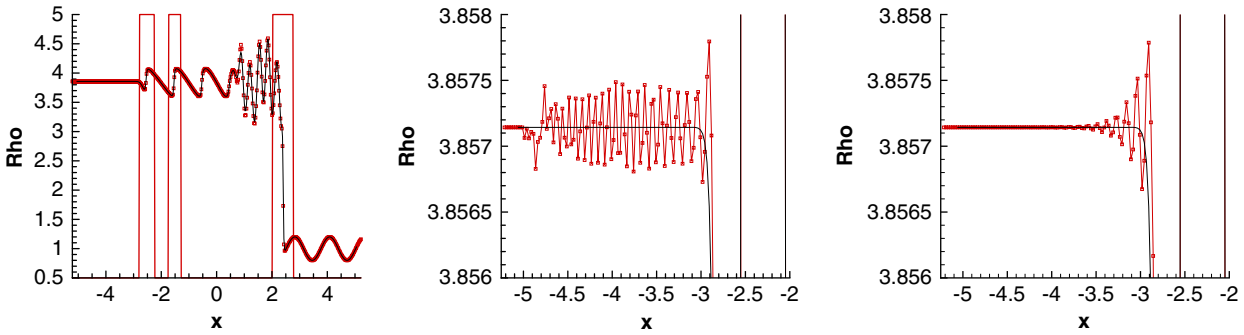

Fig. 3. Left: the density solution of the Mach 3 shock-entropy wave interaction with $N = 400$ at time $t = 1.8$. Middle: zooming of the inflow region and dispersion oscillations. Right: shows the effectiveness of the filtering in controlling the dispersion error. The solid line and the square symbols are solutions as computed by the WENO5 scheme and the Hybrid scheme, respectively.

Here ρ, m, and E are, respectively, the density, mass flux and total energy per unit volume. They are coupled with the equation of state for ideal gas, $P = (\gamma - 1)(E - 1/2m^2/\rho)$ with $\gamma = 1.4$.

Consider the one-dimensional Mach 3 shock-entropy wave interaction, specified by the following initial conditions:

$$(\rho,\ u,\ P) = \begin{cases} (3.857143, 2.629369, 10.33333), & x < -4, \\ (1 + \varepsilon \sin(kx), 0, 1), & x > -4, \end{cases} \tag{24}$$

where $x \in [-5, 5]$, $\varepsilon = 0.2$ and $k = 5$. The solution of this problem consists of not only large scales waves but also shocklets and fine scales structures which are located immediately behind the shock. We computed the solution at time $t = 1.8$ with $N = 400$ uniformly spaced grid points using both the standard fifth order WENO finite difference scheme (WENO5) and the Hybrid sixth order central finite difference-fifth order WENO finite difference scheme (Hybrid). The parameters used in the MR analysis for the Hybrid scheme are order $n_{\mathrm{MR}} = 8$, tolerance $\varepsilon_{\mathrm{MR}} = 5 \times 10^{-3}$, using the density ρ as the test function. In the left figure of Fig. 3, the solid black line and red square symbols depict the density computed with the WENO5 scheme and the Hybrid scheme, respectively. The red dash lines enclose the grid points where the solution is deemed insufficiently smooth by the MR analysis. The WENO5 scheme is employed at these grid points in order to capture the main shock and shocklets and avoid oscillations. The CeFD6 scheme is used for the rest of the grid points. At this scale, the results of the WENO5 scheme and the Hybrid scheme are in good agreement with each other.

As mentioned earlier, wave dispersion is an issue when using a non-dissipative central finite difference scheme. When zooming at the inflow region $x \in [-5, -3]$ (middle figure of Fig. 3), one observes the oscillations caused by dispersion. As proposed in last section, we apply high order filtering in order to mitigate the dispersion error. The order of the filter n_{F} used in this study is always 2 orders higher than the order of the central finite difference scheme n_{CFD}, i.e., $n_{\mathrm{F}} = n_{\mathrm{CFD}} + 2$. Furthermore, the filtering operation will be performed at the end of the Runge–Kutta time step. Filtering in the intermediate stages of the Runge–Kutta scheme is also possible if deemed necessary.

The density solution of the shock-entropy wave interaction as computed by the filtered version of the Hybrid scheme and the zooming near the inflow region are shown at the right figure of Fig. 3. It can be easily observed that the eighth order filtering improves the quality of the solution. The filter effectively controls the dispersion error and localizes the oscillations close to the steep gradients.

We now illustrate the algorithm with a longer time simulation by computing the solution up to time $t = 5$ in a larger physical domain $x \in [-5, -15]$ and $N = 800$ with both the WENO5 scheme and the Hybrid scheme with MR tolerance $\varepsilon_{\mathrm{MR}} = 10^{-2}$. Density plot, zooming of the high frequencies solution behind the main shock and the MR coefficients $\{d_j\}$ are shown at time $t = 5$ in Fig. 4. The main shock and the shocklets are well tracked and one sees that the small scales behind the main shock are better resolved with the Hybrid scheme than with the WENO5 scheme. Notice that given an appropriate threshold for the switch of the schemes, the coverage of the WENO5 scheme remains relatively quite small, indicating that the solution is mainly computed by the more efficient CeFD6 scheme. Furthermore, the decay of the MR coefficients $\{d_j\}$ near the inflow region also indicates the fast decay of the dispersion error.

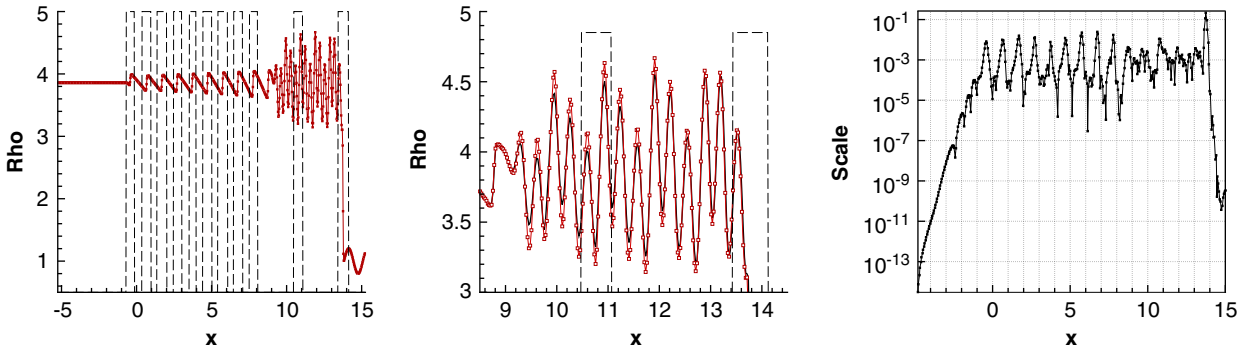

Fig. 4. Left: the density solution of the Mach 3 shock-entropy wave interaction with $N = 800$ at $t = 5$. Middle: zooming of the high frequency waves behind the main shock. Right: the multiresolution coefficients d_j at $t = 5$.

Table 1
Average CPU time (seconds) per Runge–Kutta step as a function of N

N	WENO5	Hybrid	Speedup
800	3.8e−3	1.6e−3	2.4
1000	5.1e−3	2.1e−3	2.4
1500	1.3e−2	3.2e−3	4.1
2000	2.6e−2	4.7e−3	5.5

The last column shows the speedup factor by the Hybrid scheme over the WENO5 scheme.

The Hybrid scheme has the advantage of being considerably faster than the WENO5 scheme. Even though timing of the one-dimensional system of equations is not representative as timing of a large scale simulation of a multi-dimensional system of PDEs, we provide a table listing the average CPU usage in seconds per each Runge–Kutta step of the WENO5 scheme and the Hybrid scheme just to illustrate the potential gain in computational speed. From Table 1, the gain in speed can be as much as a factor of 2 for a number of grid points $N = 800$, 1000 and up to as much as a factor of 5 for larger $N = 2000$. It is obvious that the speedup is a function of many factors such as the physical problem, the structure of the solution, the choices of the parameters, the computational platform and programming efforts. A more detailed study on the computational time of the Hybrid scheme in comparison with the standard WENO scheme will be given in a future paper.

7. Conclusions

For the high resolution solution of the nonlinear conservation laws, we have conjugated an efficient and accurate high order central finite difference scheme and the high order shock-capturing WENO finite difference scheme together to form a hybrid scheme. The spatial and temporal hybridization of these two schemes are accomplished via high order MR analysis. The numerical error due to the dispersive nature of the central finite difference scheme is controlled and localized by the employment of a high order finite difference filter, which maintains the formal high order of accuracy of the hybrid scheme. The main advantages of the hybrid scheme are the potential large reduction of CPU time needed to perform large scale numerical experiments and improvement in the overall accuracy over the classical high order WENO finite difference method. The reduction of the CPU time usage is mainly due to removal of calculations of the Jacobian of the fluxs of the PDE, the characteristic decomposition needed to project the flux from the conservative field into the characteristic field, where the WENO reconstruction of the numerical flux takes place, and back, in the smooth regions of the flow field. The improvement of the overall resolution is due to the non-dissipative nature of the central finite difference scheme that yields a better representation of the solution over the upwinding tendency of the WENO reconstruction in order to avoid using stencils with potential high gradients. The success of the hybrid scheme depends very much on the properly tuning of the parameters associated with the MR analysis and is a subject of research in progress.

Acknowledgments

The first author has been supported by CNPq, Grant 300315/98-8. The second author gratefully acknowledges the support of this work by the DOE under contract number DE-FG02-98ER25346 and AFOSR under contract number FA9550-05-1-0123. We also would like to thank Prof. David Gottlieb for his advice and discussions on this research.

References

[1] N. Adams, K. Shariff, High-resolution hybrid compact-ENO scheme for shock-turbulence interaction problems, J. Comput. Phys. 127 (1996) 27–51.
[2] D. Balsara, C.W. Shu, Monotonicity preserving weighted essentially non-oscillatory schemes with increasingly high order of accuracy, J. Comput. Phys. 160 (2000) 405–452.
[3] B. Bihari, A. Harten, Multiresolution schemes for the numerical solution of 2D Conservation Laws, SIAM J. Sci. Comput. 18 (2) (1997) 315–354.
[4] C. Bogey, C. Bailly, A family of low dispersive and low dissipative explicit schemes for flow and noise computations, J. Comput. Phys. 194 (2004) 194–214.
[5] A. Choen, S.M. Kaber, S. Muller, M. Postel, Fully adaptive multiresolution finite volume schemes for conservation laws, Math. Comput. 72 (241) (2001) 183–225.
[6] I. Daubechies, Ten Lectures on Wavelets, CBMS-NSF Regional Conferences Series in Applied Mathematics, SIAM, Capital City Press, Montpellier, Vermont, 1992.
[7] A. Harten, High resolution schemes for hyperbolic conservation laws, Comput. Phys. 49 (1983) 357–393.
[8] A. Harten, Adaptive multiresolution schemes for shock computations, Comput. Phys. 115 (1994) 319–338.
[9] A.K. Henrick, T.D. Aslam, J.M. Powers, Mapped weighted essentially non-oscillatory schemes: achieving optimal order near critical points, J. Comput. Phys. 207 (2005) 542–567.
[10] D. Hill, D. Pullin, Hybrid tuned center-difference-WENO method for large eddy simulations in the presence of strong shocks, J. Comput. Phys. 194 (2004) 435–450.
[11] G.S. Jiang, C.W. Shu, Efficient implementation of weighted ENO schemes, J. Comput. Phys. 126 (1996) 202–228.
[12] S. Pirozzoli, Conservative hybrid compact-WENO schemes for shock–turbulence interaction, J. Comput. Phys. 178 (1) (2002) 81–117.
[13] C.W. Shu, Advanced Numerical Approximation of Nonlinear Hyperbolic Equations, Lecture Notes in Mathematics, vol. 1697, Springer, Berlin, 1998, pp. 325–432.
[14] C.W. Shu, G. Erlebacher, T. Zang, D. Whitaker, S. Osher, High order ENO schemes applied to two- and three-dimensional compressible flow, Appl. Numer. Math. 9 (1992) 45–71.
[15] C.W. Shu, S. Osher, Efficient implementation of essentially non-oscillatory shock-capturing schemes, II, J. Comput. Phys. 83 (1) (1989) 32–78.
[16] O.V. Vasilyev, T.S. Lund, P. Moin, A general class of commutative filters for LES in complex geometries, J. Comput. Phys. 146 (1998) 82–104.
[17] D.W. Zingg, Comparison of high-accuracy finite difference methods for linear wave propagation, SIAM J. Sci. Comput. 22 (2) (2000) 476–502.